Heliyon 9 (2023) e23166

Contents lists available at ScienceDirect

Heliyon

journal homepage: www.cell.com/heliyon

Radiogenomics for predicting microsatellite instability status and PD-L1 expression with machine learning in endometrial cancers: A multicenter study☆

Qianling Li [a], Ya'nan Huang [b], Yang Xia [c], Meiping Li [d], Wei Tang [b], Minming Zhang [e], Zhenhua Zhao [b,*]

[a] Department of Radiology, Shaoxing People's Hospital (Shaoxing Hospital, Zhejiang University School of Medicine), Zhejiang University School of Medicine, Shaoxing, 312000, China
[b] Department of Radiology, Shaoxing People's Hospital (Shaoxing Hospital, Zhejiang University School of Medicine), Shaoxing, 312000, China
[c] Department of Radiology, Shaoxing Maternity and Child Health Care Hospital, Shaoxing, 312000, China
[d] Department of Pathology, Shaoxing Maternity and Child Health Care Hospital, Shaoxing, Zhejiang, 312000, China
[e] Department of Radiology, The Second Affiliated Hospital of Zhejiang University, Hangzhou, 310000, China

ARTICLE INFO

Keywords:
Endometrial cancer
Microsatellite instability
Mismatch repair deficiency
PD-L1
Magnetic resonance imaging
Machine learning

ABSTRACT

Purpose: To evaluate the effectiveness of machine learning model based on magnetic resonance imaging (MRI) in identifying microsatellite instability (MSI) status and PD-L1 expression in endometrial cancer (EC).

Methods: This retrospective study included 82 EC patients from 2 independent centers. Radiomics features from the intratumoral and peritumoral regions, obtained from four conventional MRI sequences (T2-weighted images; contrast-enhanced T1-weighted images; diffusion-weighted images; apparent diffusion coefficient), were combined with clinicopathologic characteristics to develop machine learning model for predicting MSI status and PD-L1 expression. 60 patients from center 1 were used as the training set for model construction, while 22 patients from center 2 were used as an external validation set for model evaluation.

Results: For predicting MSI status, the clinicopathologic model, radscore model, and combination model achieved area under the curves (AUCs) of 0.728, 0.833, and 0.889 in the training set, respectively, and 0.595, 0.790, and 0.848 in the validation set, respectively. For predicting PD-L1 expression, the clinicopathologic model, radscore model, and combination model achieved AUCs of 0.648, 0.814, and 0.834 in the training set, respectively, and 0.660, 0.708, and 0.764 in the validation set, respectively. Calibration curve analysis and decision curve analysis demonstrated good calibration and clinical utility of the combination model.

Conclusion: The machine learning model incorporating MRI-based radiomics features and clinicopathologic characteristics could be a potential tool for predicting MSI status and PD-L1 expression in EC. This approach may contribute to precision medicine for EC patients.

☆ Qianling Li and Ya'nan Huang contributed to the work equally.

* Corresponding author. Department of Radiology, Shaoxing People's Hospital (Shaoxing Hospital, Zhejiang University School), No. 568, North Zhongxing Road, Yuecheng District, Shaoxing City 312000, Zhejiang Province, China.
E-mail address: zhao2075@163.com (Z. Zhao).

https://doi.org/10.1016/j.heliyon.2023.e23166
Received 19 May 2023; Received in revised form 22 November 2023; Accepted 28 November 2023
Available online 1 December 2023

1. Introduction

Endometrial cancer (EC) is the second most commonly occurring gynecological malignancy among women globally, with a rising incidence [1,2]. The therapeutic options available for advanced or recurrent cases of EC are currently limited [3,4]. It is worth noting that patients with advanced or recurrent EC have a poor prognosis, with reported data showing an approximate 5-year survival rate of only 17 % [5].

In recent years, immunotherapy has emerged as a novel and promising treatment modality for cancer, demonstrating significant efficacy in the treatment of various solid tumors. Programmed death protein-1 (PD-1) inhibitors have emerged as a promising therapeutic option for the treatment of advanced or recurrent EC patients. Notably, the US Food and Drug Administration (FDA) has approved PD -1 immune checkpoint inhibitors for the treatment of adult patients with recurrent or advanced microsatellite unstable (MSI)/DNA mismatch repair deficiency (dMMR) EC [6,7]. This recommendation is based on clinical evidence demonstrating the efficacy of PD-1 inhibitors in improving patient outcomes, as well as the underlying biological rationale of targeting the PD-1 pathway in MSI/dMMR tumors [8]. The latest NRG-GY018 and GOG-3031 trials are global, multicenter, randomized, double-blind phase III trials, and the results of both show that the combination of immune therapy and chemotherapy for maintenance therapy (pembrolizumab and dostarlimab-gxly, two PD-1 inhibitors) can significantly improve Progression-Free Survival (PFS) in the MSI/dMMR population [9,10]. Additionally, Among gynecological malignancies, EC holds the highest occurrence of MSI/dMMR. MSI/dMMR EC is characterized by several features, including high tumor burden, increased infiltration of lymphocytes, and upregulated expression of PD-L1. Patients with these characteristics are more likely to benefit from immunotherapy [11–13].

Precision medicine has raised expectations for individualized treatments, but the research and availability of such treatments are limited by time and economic constraints [14]. To provide timely and accurate treatment options for EC patients, it is crucial to develop a rapid and prospective method for detecting immune therapy-related protein expression in EC. Radiomics is useful for capturing the characteristics of tissues and lesions. The integration of radiomics and genomics is called radiogenomics, which investigates the correlation between the two, including genomic and gene expression analysis. Radiogenomics holds great potential for predicting molecular features of tumors through easily accessible and cost-effective medical imaging [14,15].

Magnetic resonance imaging (MRI) is a commonly used imaging modality for the diagnosis of EC. With its excellent soft tissue contrast, MRI is recommended by the National Comprehensive Cancer Network (NCCN) guidelines as a preferred imaging modality for assessing the extent of local disease during the initial workup [15]. According to the International Federation of Gynecology and Obstetrics (FIGO) guidelines, MRI findings are considered the preferred criteria for staging of EC [16]. Therefore, in this study, radiomic features are extracted from four standard MRI sequences (T2WI, T2-weighted images; CE-T1WI, contrast-enhanced T1-weighted images; DWI, diffusion-weighted images; ADC, apparent diffusion coefficient). The aim of this study is to develop a machine learning model to predict DNA mismatch repair status and PD-L1 expression for optimizing the treatment of EC patients.

2. Material and methods

2.1. Patients

The Academic Ethics Committee of Shaoxing People's Hospital approved this retrospective study and waived the requirement for written informed consent from patients. A total of 82 patients diagnosed with EC were enrolled in the study, of whom 60 underwent examinations at center 1 between 2011 and 2022, and 22 underwent examinations at center 2 between 2017 and 2022. The inclusion criteria for the study were as follows:(1) Histologically confirmed EC; (2) Preoperative MRI examination; and (3) Availability of qualified postoperative pathological specimens stored in the tissue bank.

In the present study, strict exclusion criteria were applied, which included the following: (1) Administration of radiotherapy, preoperative neoadjuvant chemotherapy, or any other interventions for the lesion before MRI or surgical intervention; (2) Suboptimal image quality due to susceptible artifacts, as assessed by the experienced radiologist; (3) Incomplete MRI sequences; and (4) Presence of a lesion with a maximum diameter of less than 1 cm.

2.2. MRI protocols

Center 1: MRI imaging was performed with a 3.0 T MR scanner (Siemens Verio, Germany) and an 8-channel phased-array surface coil. Pelvic enhanced scanning was performed on all patients, with the following detailed scanning parameters: (1) T2WI: FOV: 320 × 320 mm, slice thickness: 4 mm, repetition time (TR)/echo time (TE): 4500 ms/97 ms. (2) CE-T1WI: FOV: 288 × 288 mm, slice thickness: 3 mm, TR/TE: 3.48 ms/1.3 ms. (3) DWI (b-values of 0 and 1000 s/mm^2): FOV: 160 mm × 160 mm, slice thickness: 5 mm, TR/TE: 6700 ms/92 ms. (4) ADC: FOV: 160 mm × 160 mm, slice thickness: 5 mm, TR/TE: 6700 ms/92 ms.

Center 2: MRI imaging was performed with a 1.5T MRI scanner (Siemens Avanto, Germany) and a 6-channel phased array surface coil. Pelvic-enhanced scans were performed on all patients, with the following detailed scanning parameters: (1) T2WI: FOV: 320 × 320 mm, slice thickness: 4 mm, TR/TE: 5210 ms/79 ms. (2) CE-T1WI: FOV: 320 × 320 mm, slice thickness: 4 mm, TR/TE: 735 ms/11 ms. (3) DWI (b-values of 0 and 800 s/mm^2): FOV: 160 mm × 136 mm, slice thickness: 5 mm, TR/TE:8900 ms/84 ms. (4) ADC: FOV: 160 mm × 136 mm, slice thickness: 5 mm, TR/TE: 8900 ms/84 ms.

2.3. Tumor segmentation and feature extraction

The volume of interest (VOI) for EC was delineated in four MRI sequences (T2WI, CE-T1WI, DWI, ADC) using the 3D-slicer software (version 5.2.1). Subsequently, a VOI+3 mm was generated by expanding the VOI by 3 mm and manually removing areas outside including fibroids, cysts, and fluid accumulation. Imaging features were extracted from the VOI using the AK software (Artificial Intelligent Kit, GE Healthcare, China). The image data processing settings for the two centers were as follows: normalized with the mean standard deviation as the center, resampled to a voxel size of $1 \times 1 \times 1$ mm^3 using B-spline interpolation, and a fixed bin width of 8 used in the histogram for gray dispersion.

All image segmentations were conducted by Reader 1, who had 7 years of experience in Pelvic MRI imaging. After more than one week, a subset of 30 patients was randomly selected. The image segmentation process was repeated by Reader 1, Reader 2, and Reader 3, all of whom had more than 5 years of experience in Pelvic MRI imaging. The reliability of the radiomics features was assessed using intraclass and interclass correlation coefficients (ICCs). The intra-class correlation coefficient was tested using one-way random effects, while the inter-class correlation coefficient was tested using two-way random effects combined with consistency. Radiomics features with ICCs >0.75 were retained.

2.4. Pathological examination

The determination of MSI status is based on immunohistochemistry (IHC) staining for four MMR proteins (MLH1, MSH2, PMS2, and MSH6). Tumors that exhibit nuclear staining for all four markers in at least 10 % of invasive tumor cells are classified as pMMR/microsatellite stable (MSS) (Fig. 1A), whereas those that do not meet these criteria are classified as dMMR/MSI (Fig. 1B) [17].

There is no consensus on a standardized approach for evaluating PD-L1 expression using IHC in clinical practice. Previous reports have suggested a threshold for the percentage of tumor cells stained, ranging from 1 to 10 %. PD-L1 positivity has been defined as cases with PD-L1-stained cells comprising more than 1 % of the total tumor cells (Fig. 1. C) [18], while those that do not meet these criteria are classified as negative PD-L1 expression (Fig. 1. D).

2.5. Feature selection and machine learning model construction

The feature values were normalized using Z-score normalization. Features with an absolute value of Pearson correlation coefficient ≥ 0.9 were excluded. Next, the SelectPercentile (percentile = 80) and Least Absolute Shrinkage and Selection Operator (LASSO) algorithms were used for dimensionality reduction and feature selection. Finally, logistic regression models were constructed.

The performance of the models was evaluated based on three criteria. Firstly, receiver operating characteristic (ROC) curve analysis was used to assess discriminative performance, and quantified by the corresponding AUC with 95 % confidence intervals (CIs),

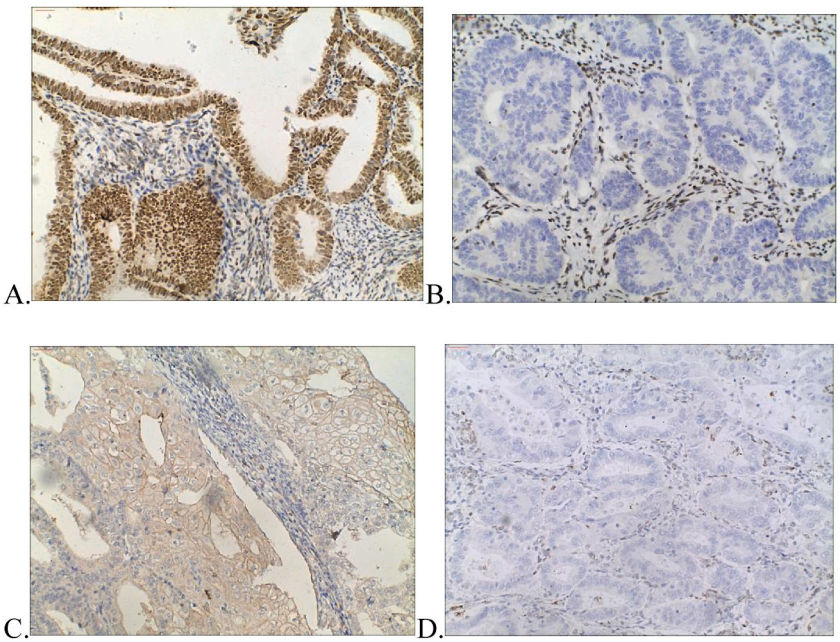

Fig. 1. Immunohistochemistry of MMR and PD-L1 in EC. Image magnification of × 200. A. A 54 years old female patient pathologically confirmed as a well differentiated EC, with pMMR. B. A 58 year old female patient pathologically confirmed as a moderately differentiated EC, with dMMR. C. A 50 years old female was diagnosed as a moderately differentiated EC with positive PD-L1 expression. D. A 49 year old female patient pathologically confirmed as a moderately differentiated EC with negative PD-L1 expression.

sensitivity, specificity, and accuracy. The AUCs were compared using Delong's test. Secondly, the calibration curve was used to measure the consistency between predicted and actual probabilities to evaluate calibration performance. Thirdly, decision curve analyses (DCA) was used to evaluate the clinical utility of the model, which quantifies the net benefit of threshold probability intervals. Radiomics feature selection and model building were performed with Python programming language version 3.7.5 (Python Software Foundation, Wilmington, DE, USA). Model evaluation, including generation of ROC curve, calibration curve, and DCA, was performed using R software version 4.2.2 (The R Foundation for Statistical Computing, Vienna, Austria). Packages and coefficients can be found in the Additional file 1. The flowchart of the study is shown in Fig. 2.

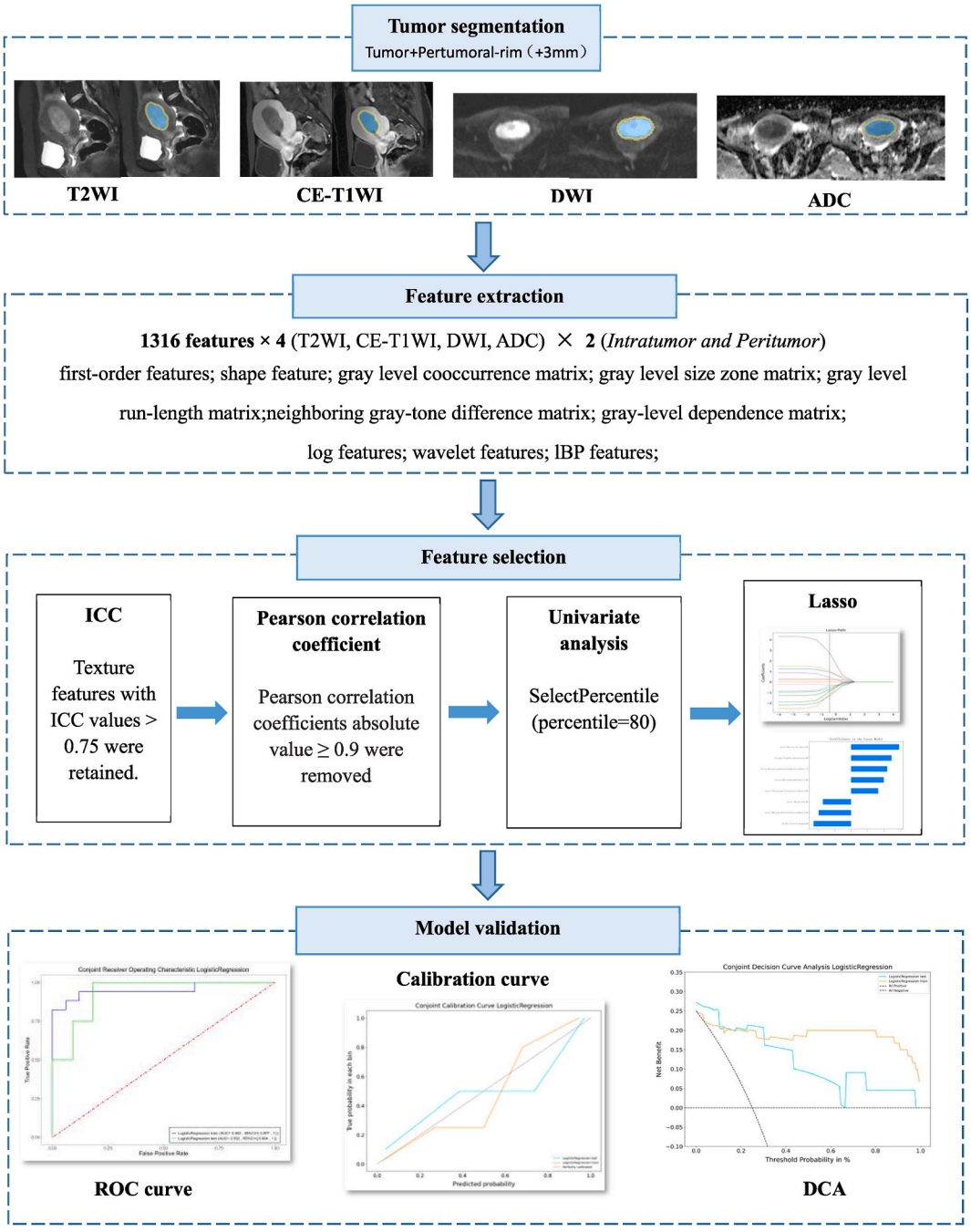

Fig. 2. Radiomic workflow including tumor segmentation, feature extraction, feature selection, model building, and model evaluation. T2WI, T2-weighted images; CE-T1WI, contrast-enhanced T1-weighted images; DWI, diffusion-weighted images; ADC, apparent diffusion coefficient; ICC, the intraclass and interclass correlation coefficient; LASSO, least absolute shrinkage, and selection operator; ROC, receiver operating characteristic; DCA, decision curve analyses.

2.6. Statistical analysis

The data were analyzed with SPSS 24.0 (Armonk, NY). The Mann-Whitney *U* test was used to analyze the continuous data (non-normally distributed values). The Chi-squared test was used for comparison between categorical variables. For all two-sided tests, a p-value of <0.05 was considered statistically significant.

3. Results

3.1. Patient

Initially, this study included 76 patients from center 1 and 55 patients from center 2. After applying exclusion criteria, a total of 82 patients were eventually enrolled in the study, with 60 patients recruited from center 1 and the remaining 22 patients recruited from center 2. Of the enrolled patients, 28 had dMMR, 54 had pMMR, 26 tested positive for PD-L1 expression, and 56 tested negative for PD-L1 expression based on IHC analysis. The patient selection process is depicted in Fig. 3.

The clinicopathologic characteristics of dMMR and pMMR tumors, as well as PD-L1-positive and PD-L1-negative tumors, are shown in Table 1. DNA mismatch repair status showed no significant differences in age, histologic type, or deep muscle infiltration ($p > 0.05$), but showed significant differences in grade and FIGO stage ($p < 0.05$). The PD-L1 expression showed no significant differences in age or histologic type ($p > 0.05$), but showed significant differences in grade, and deep muscle infiltration ($p < 0.05$).

3.2. Feature selection

A total of 10528 features were extracted, 1316 × 4 (T2WI, CE-T1WI, DWI, ADC) × 2 (Intratumor and Peritumor), which including first-order features, shape features, and texture features such as gray level co-occurrence matrix (GLCM), gray level size zone matrix (GLSZM), gray level run-length matrix (GLRLM), neighboring gray-tone difference matrix (NGTDM), gray-level dependence matrix (GLDM), log features, wavelet features, and local binary pattern (LBP) features.

Of the 10528 radiomic features extracted from the MRI images, 7125 features were found to be stable (ICC≥0.75). For the model predicting MSI status, feature selection was performed based on Pearson correlation, removing features with an absolute Pearson correlation coefficient≥0.9. After univariate feature selection (SelectPercentile), 623 features were retained, and then the LASSO algorithm was used to select the 8 most valuable radiomic features from the training set. The radiomic score was calculated for each

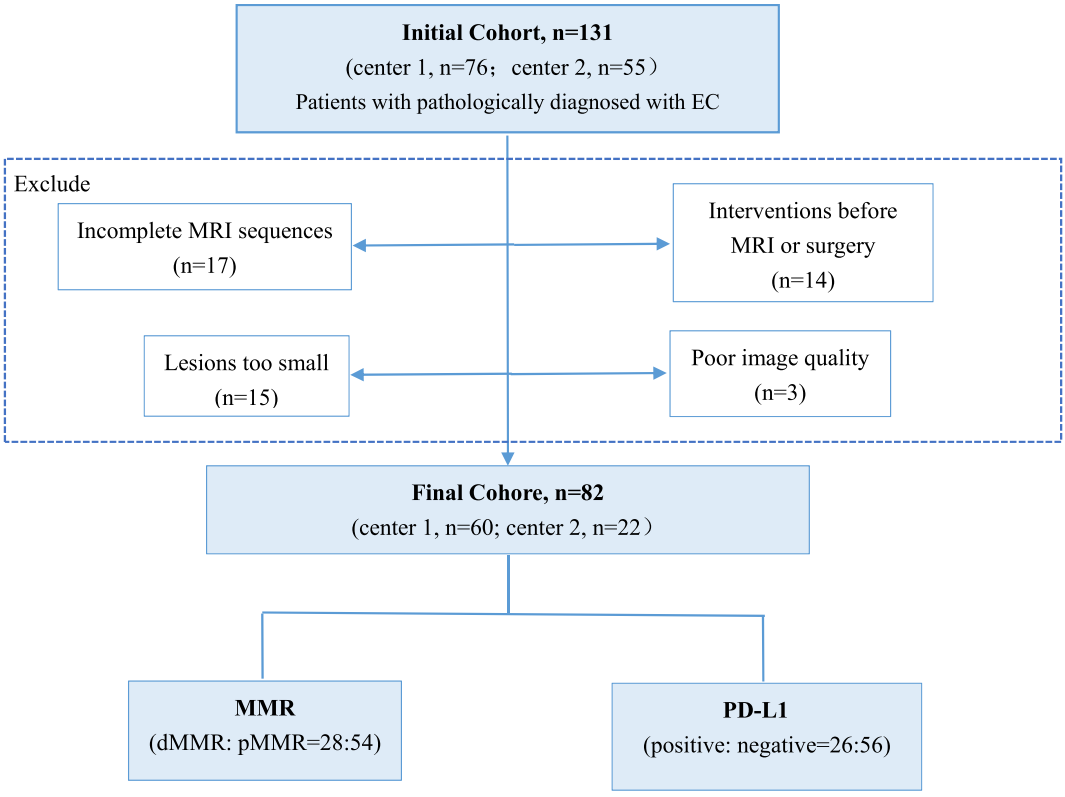

Fig. 3. Workflow shows the selection of the studying population and exclusion criteria.

Table 1
Clinicopathological parameters and DNA mismatch repair status, PD-L1 status.

	DNA mismatch repair status		p value	PD-L1 status		p value
	pMMR N(%)	dMMR N(%)		negative N(%)	positive N(%)	
Total	54 (65.9)	28 (34.1)		56 (68.3)	26 (31.7)	
Age	59.37 ± 9.57	58.75 ± 9.64	0.78	59.07 ± 9.82	59.32 ± 9.13	0.91
Histologic type						
EEC	49 (59.8)	26 (31.7)	1.00	50 (61.0)	25 (30.5)	0.62
Non-EEC	5 (6.1)	2 (2.4)		6 (7.3)	1 (1.2)	
Grade						
I	42 (51.2)	11 (13.4)	<0.01*	46 (37.8)	7 (15.8)	<0.01*
II/III	12 (14.6)	17 (20.7)		10 (28.0)	19 (18.3)	
Deep muscle infiltration						
-	45 (54.9)	20 (24.4)	0.21	49 (59.8)	16 (19.5)	<0.01*
+	9 (11.0)	8 (9.8)		7 (8.5)	10 (12.2)	
FIGO stage						
I-II	53 (64.6)	23 (28.0)	0.03*	54 (65.9)	22 (26.8)	0.15
III-IV	1(1.2)	5 (6.1)		2 (2.4)	4 (4.9)	

*$p < 0.05$, significant. Continuous variables were presented as mean ± standard deviation, while categorical variables were reported as patient numbers with percentages in parentheses. EEC, Endometrioid Endometrial Carcinoma; FIGO, International Federation of Gynecology and Obstetrics; dMMR, deficient mismatch repair; pMMR, proficient mismatch repair.

patient using the 8 nonzero coefficient features and used to construct the prediction model. For the PD-L1 expression prediction model, features were selected similarly based on Pearson correlation, with those having an absolute Pearson correlation coefficient $\geq$0.9 removed. After univariate feature selection (SelectPercentile), 440 features were retained, and then the LASSO algorithm was used to select the 8 most valuable radiomic features from the training set. The radiomic score was calculated using the 8 nonzero coefficient features and used to construct the prediction model. The selected features and their descriptions are shown in Table 2. The formula for calculating the rad-score and the corresponding feature weighting diagram are included in Additional file 2.

3.3. The predictive power of machine learning models

The performance of the clinicopathologic, radscore, and combination predictive models for EC MSI status and PD-L1 expression was evaluated using ROC curves. The AUCs of models (clinicopathologic, radscore, and combination) for predicting MSI status in the training set (Fig. 4 A) and validation set (Fig. 4 B) were 0.728, 0.833, 0.889, and 0.595, 0.790, 0.848, respectively. The AUC of models (clinicopathologic, radscore, and combination) for predicting PD-L1 expression in the training set (Fig. 4 C) and validation set (Fig. 4 D) was 0.648, 0.814, 0.834, and 0.660, 0.708, 0.764, respectively. The AUC, sensitivity, specificity, and accuracy values are presented in Table 3. Delong's test was used to compare the differences in AUC between the models, and the results are shown in Table 4 $p < 0.05$ indicates statistical significance. Calibration curve analysis (Fig. 5A–D) and DCA (Fig. 6A–D) were conducted on both the training and validation set, revealing favorable calibration and clinical applicability.

4. Discussion

The aim of the study was to develop a machine learning model for predicting genetic information, MSI status and PD-L1 expression, in EC patients by using four conventional MRI sequences and clinicopathological features. Previous research in the field of radiogenomics has demonstrated the feasibility of using imaging data to predict clinically relevant molecular profiles in various cancers, including breast cancer, lung cancer, glioblastoma, and pancreatic cancer [19–22]. In this study, the machine learning model based on MR multi-sequence imaging and clinicopathological features has also demonstrated good discrimination efficiency in predicting the MSI status and PD-L1 expression of EC, as well as good adaptability and clinical effectiveness.

To our knowledge, limited research has been conducted on the use of radiomics-based methods for evaluating genetic information related to MSI status in EC according to current medical literature, and no studies have been carried out to predict PD-L1 expression. A previous study has used intratumoral radiomic features based on T1 and T2 MRI sequences to predict MSI status in EC [23]. However, this study did not take into account the radiomic features from the tumor margin. Numerous studies across multiple tumor types have reported the value of radiomics of the tumor margin in revealing correlations with tumor biology, prognosis, and treatment response [24–30]. In this study, the machine learning model was constructed by combining intratumoral and peritumoral radiomic features. Significantly, our findings demonstrated that the peritumoral features contributed more to the combination model compared to the intratumoral features, which is consistent with the findings of Harini Veeraraghavan et al. [31]. Several studies have demonstrated the correlation between radiomic features of the tumor margin and tumor infiltrating lymphocyte (TIL) density in breast cancer [25,28]. In addition, it is also known that the composition of tumor TILs is higher in dMMR tumors than in pMMR tumors [32,33]. Therefore, we speculate that the greater contribution of peritumoral radiomic features to the model may be related to the significant lymphocytic infiltration around dMMR tumors. Furthermore, two additional sequences, DWI and ADC, were included in this study compared with previous studies, which are also of greater value for EC typing, grading, and staging.

Previous studies have reported a prevalence of dMMR in EC ranging from 25 % to 31 % [8,34]. In our study, we observed that

Table 2
Selected features of the models.

Model	Feature name	Description
MSI	Wavelet-HLL_firstorder_Maxinmum_T1WI_peritumor	The maximum gray level intensity of the ROI
	Log-sigma-3-0-mm-3D_gldm_LowGrayLevelEmphasis_T2WI_peritumor	The distribution of low gray-level values
	Lbp-3D-k_glcm_ClusterShade_DWI_peritumor	The skewness and uniformity measurement
	Log-sigma-2-0-mm-3D_firstorder_Maxinmum_T1WI_peritumor	The maximum gray level intensity of the ROI
	Original_glcm_Correlation_T2WI_peritumor	The linear dependency of gray level values to their respective voxels
	Wavelet-LLH_glszm_GrayLevelNonUniformityNormalized_DWI_intratumor	The variability of gray-level intensity values in the image
	Wavelet-LLH_glszm_SmallAreaEmphasis_DWI_peritumor	The distribution of small size zones
	Original_glcm_Imc_T2WI_peritumor	The correlation between the probability distributions
PD-L1	Wavelet-HHH_firstorder_Kurtosis_DWI_peritumor	The "peakedness" of the distribution of values in the image ROI.
	Log-sigma-2-0-mm-3D_gldm_DependenceNonUniformityNormalized_DWI_peritumor	The similarity of dependence throughout the image
	Wavelet-HHL_glszm_SizeZoneNonUniformityNormalized_T2WI_peritumor	The variability of size zone volumes
	Wavlet-HHH_glszm_SmallAreaLowGrayLevelEmphasis_DWI_intratumor	The proportion in the image of the joint distribution of smaller size zones with lower gray-level values
	Lbp-3D-k_firstorder_Kurtosis_ADC_peritumor	The "peakedness" of the distribution of values in the image ROI.
	Wavelet-HLL_firstorder_Skewness_DWI_peritumor	The asymmetry of the mean value
	Wavelet-HLL_firstorder_Skewness_T2WI_intratumor	The asymmetry of the mean value
	Wavelet-HLH_glszm_SizeZoneNonUniformityNormalized_T1WI_intratumor	The variability of size zone volumes

T1WI, T1-weighted images; T2WI, T2-weighted images; DWI, Diffusion-weighted images; ADC, Apparent diffusion coefficien.

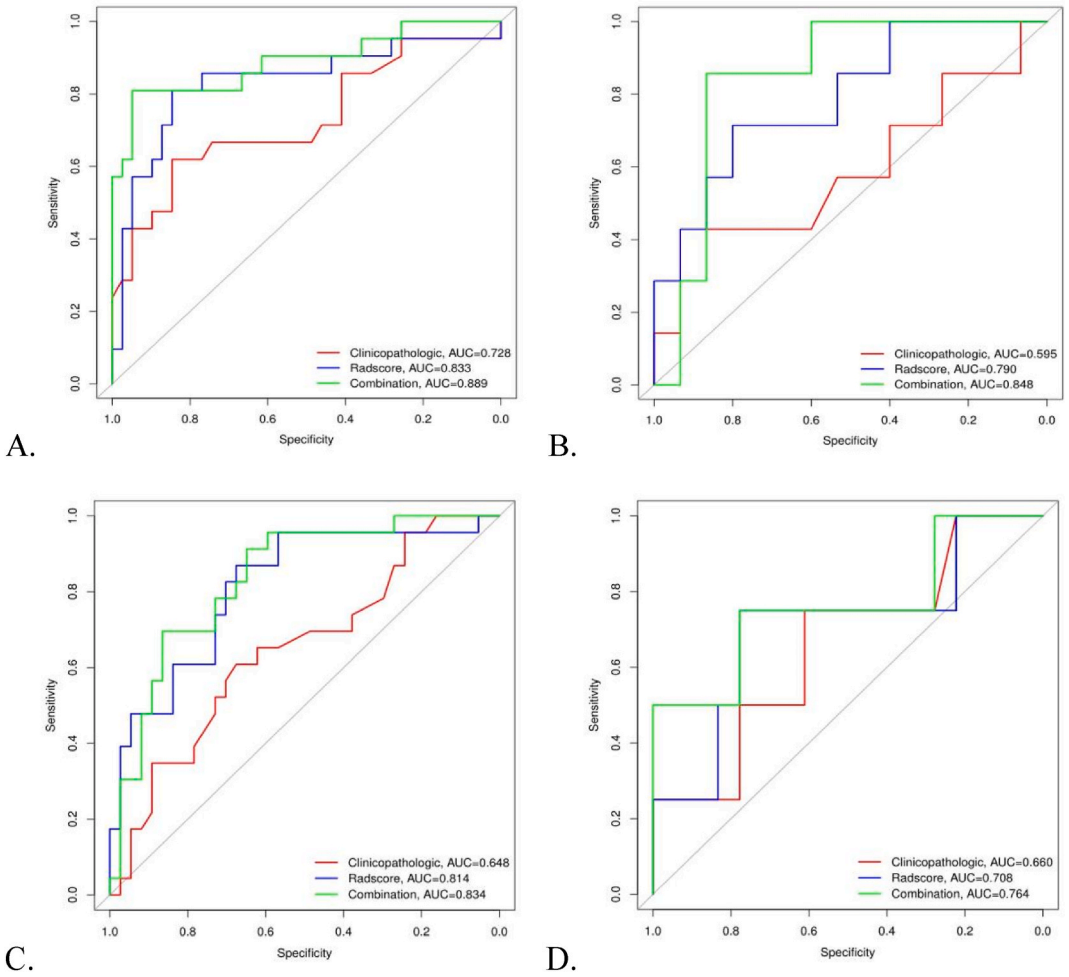

Fig. 4. The ROC curves to predict MSI status in the training (A) and validation set (B). The ROC curves to predict PD-L1 expression in the training set (C) and validation set (D). A. B. C.D.

Table 3
The predictive performance of the models.

	Model	Training set				Validation set			
		AUC (95 % CI)	SEN	SPE	ACC	AUC (95 % CI)	SEN	SPE	ACC
MSI	Clinicopathologic	0.728 (0.597–0.835)	0.619	0.846	0.767	0.595 (0.368–0.796)	0.429	0.733	0.636
	Radscore	0.833 (0.714–0.917)	0.810	0.846	0.833	0.790 (0.566–0.932)	0.286	0.933	0.727
	Combination	0.889 (0.781–0.955)	0.810	0.949	0.900	0.848 (0.632–0.963)	0.429	0.867	0.727
PD-L1	Clinicopathologic	0.648 (0.514–0.767)	0.609	0.676	0.650	0.660 (0.429–0.845)	0.750	0.556	0.591
	Radscore	0.814 (0.693–0.903)	0.870	0.676	0.750	0.708 (0.478–0.880)	0.750	0.500	0.546
	Combination	0.834 (0.716–0.918)	0.913	0.649	0.750	0.764 (0.537–0.916)	0.750	0.333	0.410

AUC, the area under the curve; SEN, sensitivity; SPE, specificity; ACC, accuracy; CI, confidence interval.

Table 4
Results of the Delong's test.

Model	MSI		PD-L1	
	Training	Validation	Training	Validation
Combination vs Radscore	0.135	0.494	0.449	0.341
Combination vs Clinicopathologic	0.030*	0.096	0.006*	0.696
Radscore vs Clinicopathologic	0.227	0.257	0.051	0.866

*$p < 0.05$, significant.

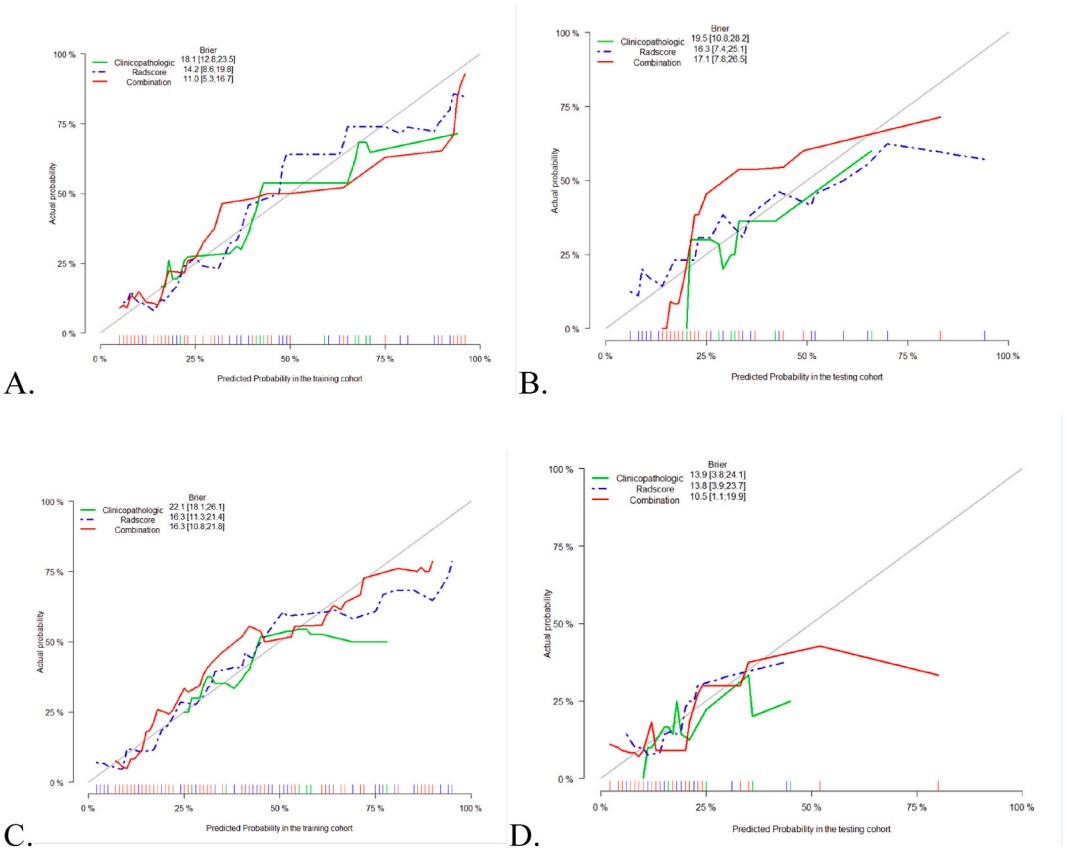

Fig. 5. Calibration curves of the prediction models that predict the MSI status in the training set (A) and validation set (B). Calibration curves of the prediction models that predict the PD-L1 expression in the training set (C) and validation set (D).
The gray line is the ideal calibration curve when the predicted value is equal to the actual value. The closer the model calibration curve is to this line, the better the prediction ability of this model is.

approximately 34.1 % of EC cases exhibited dMMR, which is similar to the findings of previous studies. The most extensive study to date regarding PD-L1 expression in EC encompassed 700 patients and found that PD-L1 expression occurred in approximately 30 % of dMMR tumors and less than 5 % of pMMR tumors. Other studies reported even higher rates of PD-L1 expression, up to 53 %, in dMMR tumors [35,36]. In our study, we observed that 65.4 % of dMMR EC cases displayed positive PD-L1 expression, whereas 20.3 % of pMMR cases demonstrated PD-L1 positivity. These results suggest a greater frequency of PD-L1 expression than those documented in prior studies. Nevertheless, it is important to note that all above studies consistently found higher expression of PD -L1 in dMMR cases compared with pMMR cases. The discrepancies in reported percentages can likely be attributed to methodological differences and variations in the threshold for determining positivity. McMeekin et al. analyzed clinical data from 1024 cases of endometrial endometrioid carcinoma (EEC) and found that EEC with dMMR was associated with poor prognostic factors such as advanced FIGO stage and high tumor grade. The study confirmed this correlation and also found that PD-L1 expression was correlated with high tumor grade, and deep muscle infiltration. Interestingly, this experiment revealed no significant correlation between DNA mismatch repair status and the histologic type of EC. Although this finding is consistent with the conclusions of previous studies by Zijing Lin et al. [23], it should be noted that our experiment had a relatively small sample size. Therefore, further validation with larger datasets is required to confirm this observation. MMR IHC and PD-L1 IHC are valuable techniques for the accurate determination of DNA mismatch repair status and PD-L1 expression. However, they are highly influenced by technical and subjective factors, moreover, IHC is generally performed only focally. In this study, a machine learning method is proposed. This method has the potential to overcome the limitations of focal IHC and provide a more comprehensive evaluation of lesions.

Our study has several limitations. Firstly, due to the small size of our patient cohort and the retrospective nature of the study, while the proposed model has been validated in an external dataset, larger prospective validation is still needed to verify the robustness of our model before implementation in clinical practice. Secondly, utilizing deep learning algorithms can further enhance radiogenomics analysis. Deep learning can identify significant features without the need for segmentation, and its performance is superior to traditional machine learning methods based on “hand-crafted” features, given sufficient training data [37]. Thirdly, due to the variations in MR imaging parameters and MRI vendors, the heterogeneity exhibited in our study potentially impacts the extracted radiomics feature values and model performance, although each patient scan was normalized to obtain a standard distribution of

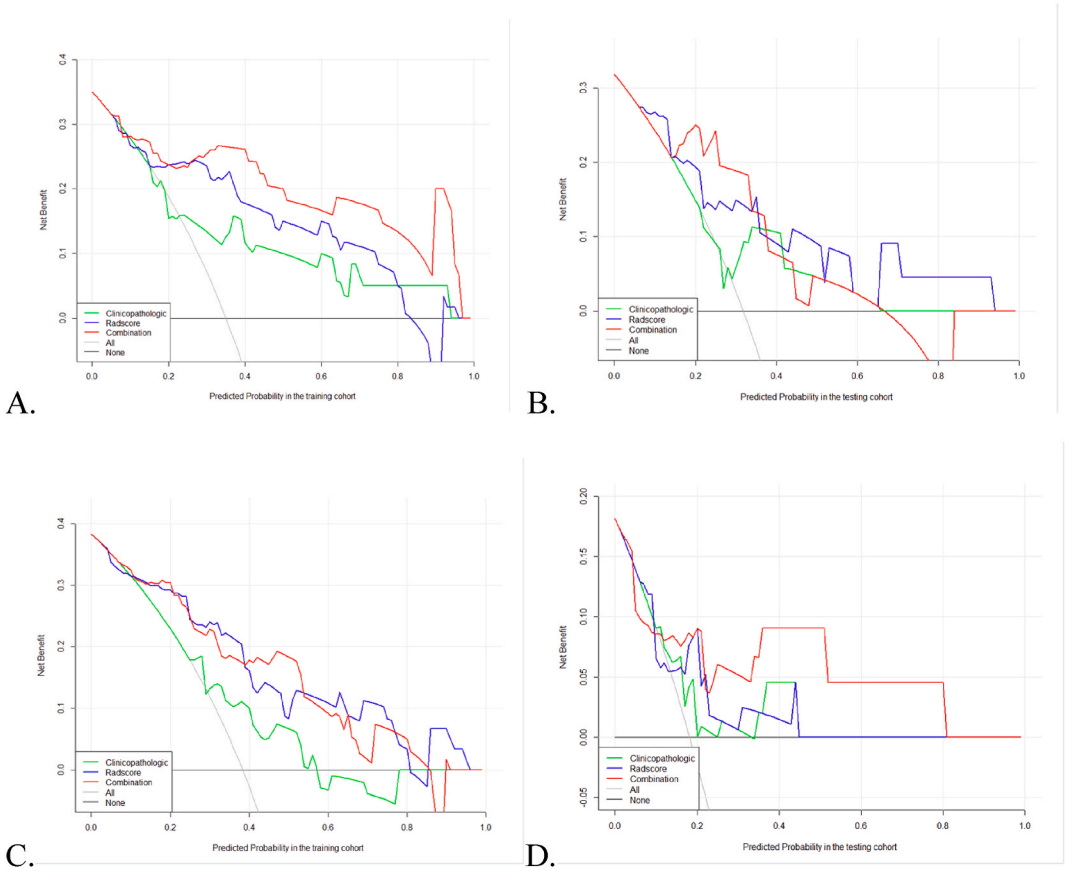

Fig. 6. Decision curve analyses of the prediction models that predict the MSI status in the training set (A) and validation set (B). Decision curve analyses of the prediction models that predict the PD-L1 expression in training set (C) and validation set (D).
The abscissa represents the risk of disease occurrence, the ordinate represents the patient's net income rate, and the gray curve represents that all patients have adverse outcomes. When the prediction model curve is above the gray curve, it represents that the corresponding patients can benefit.

image intensities to reduce heterogeneity, here is still a need for further improvements to ensure feature reproducibility. Finally, our study mainly included early-stage primary EC cases. Given that pembrolizumab and dostarlimab-gxly have currently been approved by the FDA for advanced or recurrent diseases, it will be important to validate our results in advanced disease settings.

5. Conclusion

In the field of precision medicine for EC, the application of MRI-based machine learning models represents a promising tool for predicting MSI status and PD-L1 expression. This approach could contribute to the implementation of immunotherapy for EC patients and ultimately improve treatment outcomes in the future.

Data availability statement

Because the information comes from the hospital case system, the data sets generated and analyzed during the current study period are not publicly available, but can be obtained from the corresponding authors on reasonable request.

Ethics statement

This study was reviewed and approved by The Academic Ethics Committee of Shaoxing People's Hospital, with the approval number: [shaoshiyilunshen-2023-yanli No. 044-Y-01].

Informed consent was not required for this study because it was a retrospective study conducted with existing data without direct interaction with individuals. The data used in the study were anonymized and did not involve any new interventions or risks.

Funding disclosure

This study in part by grants from the Shaoxing Health and Technology Plan Project (2022SY008), the General Plan for Medical and Health Research in Zhejiang (2021KY371), and the institution from Key Laboratory of Functional Molecular Imaging of Tumor and Interventional Diagnosis and Treatment of Shaoxing City (Shaoxing People's Hospital, Shaoxing, Zhejiang, China, grant number, 2020ZDSYSO1).

Declarations

The patients whose images are included in this publication have consented to the publication of these images.

CRediT authorship contribution statement

Qianling Li: Writing – original draft, Methodology, Investigation. **Ya'nan Huang:** Methodology, Data curation. **Yang Xia:** Resources. **Meiping Li:** Resources. **Wei Tang:** Data curation. **Minming Zhang:** Supervision, Methodology. **Zhenhua Zhao:** Supervision, Resources, Project administration, Methodology, Funding acquisition.

Declaration of competing interest

The authors declare that they have no known competing financial interests or personal relationships that could have appeared to influence the work reported in this paper.

Appendix A. Supplementary data

Supplementary data to this article can be found online at https://doi.org/10.1016/j.heliyon.2023.e23166.

References

[1] F. Bray, J. Ferlay, I. Soerjomataram, et al., Lobal cancer statistics 2018: GLOBOCAN estimates of incidence and mortality worldwide for 36 cancers in 185 countries, CA Cancer J Clin 68 (6) (2018) 394–424, https://doi.org/10.3322/caac.21492.
[2] S. Zhang, T.T. Gong, F.H. Liu, et al., Global, regional, and national burden of endometrial cancer, 1990-2017: results from the global burden of disease study, 2017, Front Oncol 9 (2019) 1440, https://doi.org/10.3389/fonc.2019.01440.
[3] N. Abu-Rustum, C. Yashar, K. Bradley, et al., NCCN Guidelines® insights: uterine neoplasms, version 3.2021, J. Natl. Compr. Canc. Netw. 19 (8) (2021) 888–895, https://doi.org/10.6004/jnccn.2021.0038.
[4] G.F. Fleming, Second-line therapy for endometrial cancer: the need for better options, J. Clin. Oncol. 33 (31) (2015) 3535–3540, https://doi.org/10.1200/JCO.2015.61.7225.
[5] R.L. Siegel, K.D. Miller, H.E. Fuchs, et al., Cancer statistics, CA Cancer J Clin 71 (2021) 7–33, https://doi.org/10.3322/caac.21654.
[6] M.N. Mamat Yusof, K.T. Chew, N. Kampan, et al., PD-L1 expression in endometrial cancer and its association with clinicopathological features: a systematic review and meta-analysis, Cancers 14 (16) (2022) 3911, https://doi.org/10.3390/cancers14163911.
[7] H. Yamashita, K. Nakayama, M. Ishikawa, et al., Microsatellite instability is a biomarker for immune checkpoint inhibitors in endometrial cancer, Oncotarget 9 (5) (2017) 5652–5664, https://doi.org/10.18632/oncotarget.23790.
[8] D.M. O'Malley, G.M. Bariani, P.A. Cassier, et al., Pembrolizumab in patients with microsatellite instability-high advanced endometrial cancer: results from the KEYNOTE-158 study, J. Clin. Oncol. 40 (7) (2022) 752–761, https://doi.org/10.1200/JCO.21.01874.
[9] R.N. Eskander, M.W. Sill, L. Beffa, et al., Pembrolizumab plus chemotherapy in advanced endometrial cancer, N. Engl. J. Med. 388 (23) (2023) 2159–2170, https://doi.org/10.1056/NEJMoa2302312.
[10] M.R. Mirza, D.M. Chase, B.M. Slomovitz, et al., Dostarlimab for primary advanced or recurrent endometrial cancer, N. Engl. J. Med. 388 (23) (2023) 2145–2158, https://doi.org/10.1056/NEJMoa2216334.
[11] Z. Li, A.S. Joehlin-Price, J. Rhoades, et al., Parwani Programmed death ligand 1 expression among 700 consecutive endometrial cancers: strong association with mismatch repair protein deficiency, Int. J. Gynecol. Cancer 28 (2018) 59–68, https://doi.org/10.1097/IGC.0000000000001120.
[12] D.T. Le, J.N. Durham, K.N. Smit, et al., Mismatch repair deficiency predicts response of solid tumors to PD-1 blockade, Science 357 (6349) (2017) 409–413, https://doi.org/10.1126/science.aan6733.
[13] G. Mittica, E. Ghisoni, G. Giannone, et al., Checkpoint inhibitors in endometrial cancer: preclinical rationale and clinical activity, Oncotarget 8 (52) (2017) 90532–90544, https://doi.org/10.18632/oncotarget.20042.
[14] S.S. Yip, H.J. Aerts, Applications and limitations of radiomics, Phys. Med. Biol. 61 (13) (2016) R150–R166, https://doi.org/10.1088/0031-9155/61/13/R150.
[15] C. Herskind, C.J. Talbot, S.L. Kerns, , et al.West CM. Radiogenomics, A systems biology approach to understanding genetic risk factors for radiotherapy toxicity, Cancer Lett. 382 (1) (2016) 95–109, https://doi.org/10.1016/j.canlet.2016.02.035.
[16] W.J. Koh, N.R. Abu-Rustum, S. Bean, et al., Uterine neoplasms, version 1. 2018, NCCN clinical practice guidelines in oncology, J Natl Compr Canc Netw 16 (2) (2018) 170–199, https://doi.org/10.6004/jnccn.2018.0006.
[17] F. Dedeurwaerdere, K.B. Claes, J. Van Dorpe, et al., Comparison of microsatellite instability detection by immunohistochemistry and molecular techniques in colorectal and endometrial cancer, Sci. Rep. 11 (1) (2021), 12880, https://doi.org/10.1038/s41598-021-91974-x.
[18] H.L. Gao, L. Liu, Z.H. Qi, et al., The clinicopathological and prognostic significance of PD-L1 expression in pancreatic cancer: a meta-analysis, Hepatobiliary Pancreat. Dis. Int. 17 (2) (2018) 95–100, https://doi.org/10.1016/j.hbpd.2018.03.007.
[19] G.A. Woodard, K.M. Ray, B.N. Joe, et al., Qualitative radiogenomics: association between oncotype DX test recurrence score and BI-rads mammographic and breast MR imaging features, Radiology 286 (1) (2018) 60–70, https://doi.org/10.1148/radiol.2017162333.
[20] M. Zhou, A. Leung, S. Echegaray, et al., Non-small cell lung cancer radiogenomics map identifies relationships between molecular and imaging phenotypes with prognostic implications, Radiology 286 (1) (2018) 307–315, https://doi.org/10.1148/radiol.2017161845.
[21] P. Kickingereder, D. Bonekamp, M. Nowosielski, et al., Radiogenomics of glioblastoma: machine learning-based classification of molecular characteristics by using multiparametric and multiregional MR imaging features, Radiology 281 (3) (2016) 907–918, https://doi.org/10.1148/radiol.2016161382.

[22] Y. Iwatate, I. Hoshino, H. Yokota, et al., Radiogenomics for predicting p53 status, PD-L1 expression, and prognosis with machine learning in pancreatic cancer, Br. J. Cancer 123 (8) (2020) 1253–1261, https://doi.org/10.1038/s41416-020-0997-1.
[23] Z. Li, T. Wang, H. Li, et al., Magnetic resonance-based radiomics nomogram for predicting microsatellite instability status in endometrial cancer, Quant Imaging Med Surg 13 (1) (2023) 108–120, https://doi.org/10.21037/qims-22-255.
[24] N. Braman, P. Prasanna, J. Whitney, et al., Association of peritumoral radiomics with tumor biology and pathologic response to preoperative targeted therapy for HER2 (ERBB2)-Positive breast cancer, JAMA Netw. Open 2 (4) (2019), e192561, https://doi.org/10.1001/jamanetworkopen.2019.2561.
[25] T.H. Dou, T.P. Coroller, J.J.M. van Griethuysen, et al., Peritumoral radiomics features predict distant metastasis in locally advanced NSCLC, PLoS One 13 (11) (2018), e0206108, https://doi.org/10.1371/journal.pone.0206108.
[26] M. Khorrami, P. Jain, K. Bera, et al., Predicting pathologic response to neoadjuvant chemoradiation in resectable stage III non-small cell lung cancer patients using computed tomography radiomic features, Lung Cancer 135 (2019) 1–9, https://doi.org/10.1016/j.lungcan.2019.06.020.
[27] N.M. Braman, M. Etesami, P. Prasanna, et al., Intratumoral and peritumoral radiomics for the pretreatment prediction of pathological complete response to neoadjuvant chemotherapy based on breast DCE-MRI, Breast Cancer Res. 19 (1) (2017) 57, https://doi.org/10.1186/s13058-017-0846-1.
[28] N. Beig, M. Khorrami, M. Alilou, et al., Perinodular and intranodular radiomic features on lung CT images distinguish adenocarcinomas from granulomas, Radiology 290 (3) (2019) 783–792, https://doi.org/10.1148/radiol.2018180910.
[29] P. Prasanna, J. Patel, S. Partovi, et al., Radiomic features from the peritumoral brain parenchyma on treatment-naïve multi-parametric MR imaging predict long versus short-term survival in glioblastoma multiforme: preliminary findings, Eur. Radiol. 27 (10) (2017) 4188–4197, https://doi.org/10.1007/s00330-016-4637-3.
[30] X. Xu, H.L. Zhang, Q.P. Liu, et al., Radiomic analysis of contrast-enhanced CT predicts microvascular invasion and outcome in hepatocellular carcinoma, J. Hepatol. 70 (6) (2019) 1133–1144, https://doi.org/10.1016/j.jhep.2019.02.023.
[31] H. Veeraraghavan, C.F. Friedman, D.F. DeLair, et al., Machine learning-based prediction of microsatellite instability and high tumor mutation burden from contrast-enhanced computed tomography in endometrial cancers, Sci. Rep. 10 (1) (2020), 17769, https://doi.org/10.1038/s41598-020-72475-9.
[32] J.B. Pakish, Q. Zhang, Z. Chen, et al., Immune microenvironment in microsatellite-instable endometrial cancers: hereditary or sporadic origin matters, Clin. Cancer Res. 23 (15) (2017) 4473–4481, https://doi.org/10.1158/1078-0432.CCR-16-2655.
[33] S. Narayanan, T. Kawaguchi, X. Peng, et al., Tumor infiltrating lymphocytes and macrophages improve survival in microsatellite unstable colorectal cancer, Sci. Rep. 9 (1) (2019), 13455, https://doi.org/10.1038/s41598-019-49878-4.
[34] N.A.J. Ryan, M.A. Glaire, D. Blake, et al., The proportion of endometrial cancers associated with Lynch syndrome: a systematic review of the literature and meta-analysis, Genet. Med. 21 (10) (2019) 2167–2180, https://doi.org/10.1038/s41436-019-0536-8.
[35] E.A. Sloan, K.L. Ring, B.C. Willis, et al., PD-L1 expression in mismatch repair-deficient endometrial carcinomas, including lynch syndrome-associated and MLH1 promoter hypermethylated tumors, Am. J. Surg. Pathol. 41 (3) (2017) 326–333, https://doi.org/10.1097/PAS.0000000000000783.
[36] N. Sungu, M. Yildirim, R. Desdicioglu, et al., Expression of immunomodulatory molecules PD-1, PD-L1, and PD-L2, and their relationship with clinicopathologic characteristics in endometrial cancer, Int. J. Gynecol. Pathol. 38 (5) (2019) 404–413, https://doi.org/10.1097/PGP.0000000000000543.
[37] A. Hosny, C. Parmar, J. Quackenbush, et al., Artificial intelligence in radiology, Nat. Rev. Cancer 18 (8) (2018) 500–510, https://doi.org/10.1038/s41568-018-0016-5.